https://doi.org/10.5194/egusphere-2026-1446
Preprint. Discussion started: 30 March 2026

The role of the secondary circulation in the tropical transition of Hurricane Ophelia

Carlos Calvo-Sancho[1]*, Richard Rotunno[2], Ana Montoro-Mendoza[3,4], Mauricio López-Reyes[5,6,7], Juan Jesús González-Alemán[3], Pedro Bolgiani[6], María Luisa Martín[3,8]

[1] Centro de Investigaciones sobre Desertificación, Consejo Superior de Investigaciones Científicas (CIDE, CSIC-UV-GVA), Climate, Atmosphere and Ocean Laboratory (Climatoc-Lab), Moncada, Valencia, Spain.

[2] NSF National Centre for Atmospheric Research (NCAR), Boulder, Colorado, US.

[3] Agencia Estatal de Meteorología (AEMET). Spain.

[4] Department of Applied Mathematics. Faculty of Computer Engineering, Universidad de Valladolid, Spain.

[5] Instituto de Astronomía y Meteorología (IAM), Centro Universitario de Ciencias Exactas e Ingenierías (CUCEI), Departamento de Física, Universidad de Guadalajara, Guadalajara, México.

[6] Department of Earth Physics and Astrophysics. Faculty of Physics, Universidad Complutense de Madrid, Spain.

[7] Instituto Frontera A.C., Departamento de Investigación, Tijuana, México.

[8] Interdisciplinary Mathematics Institute. Universidad Complutense de Madrid, Spain.

Correspondence to: Carlos Calvo-Sancho (carlos.calvo@csic.es)

Abstract. This study investigates the mesoscale dynamic and thermodynamic mechanisms governing the tropical transition (TT) of Hurricane Ophelia (2017). A fundamental aspect of this transition is the co-evolution of the primary and secondary circulations; specifically, the development of the secondary overturning circulation is what drives the structural evolution of the vortex. As the first high-resolution analysis of secondary circulation in a real TT, it broadens the scope of existing diagnostic frameworks, proving that methods originally developed for idealized tropical cyclones are also effective for quantifying the dynamics of transitioning systems. Using high-resolution numerical simulations, advanced energy-budget diagnostics and wind-tendency equations have been computed to assess the evolution of the secondary circulation. Results show that following an initial phase driven by an upper-level potential vorticity intrusion and baroclinic forcing, organized deep convection facilitates vorticity redistribution and core warming. During the transition phase, momentum and thermal forcings contribute nearly equally to the intensification of the secondary circulation. However, once the transition is complete, thermal forcing becomes the dominant mechanism. The equivalent potential temperature budget analysis reveals a fundamental shift in system energetics: while vertical diffusion, associated with surface fluxes and air-sea instability, dominates energy input during the transition, organized vertical advection within the eyewall sustains the system in its mature stage. The study also identifies a period of structural relaxation midway through the process, highlighting the non-linear nature of the tropical transition before achieving self-sustaining convective coupling. By clarifying currently debated TT behavior, this work establishes key signatures that facilitate the non-trivial characterization of these systems.

1 Introduction

Tropical transition (TT) represents a significant pathway for tropical cyclone (TC) formation, accounting for 10–20% of all named systems in the North Atlantic (NATL; Davis and Bosart, 2003; McTaggart-Cowan et al., 2013). These events typically occur when non-tropical baroclinic systems evolve into warm-core TCs, a process of increasing relevance in subtropical and midlatitude environments (Guishard et al., 2009; Kossin et al., 2014; Montoro-Mendoza et al., 2024, 2026a). Even though they are becoming more important in subtropical and midlatitude areas, especially in the NATL (Guishard et al., 2009; Kossin et al., 2014; Montoro-Mendoza et al., 2024, 2026), and despite substantial progress, key uncertainties remain regarding the dynamic and thermodynamic processes governing TT (Cao et al., 2025; Kossin et al., 2014; Vecchi and Knutson, 2008; Walsh et al., 2019). The evolution of a TT is driven by the interaction between baroclinic forcing, often initiated by upper-level potential vorticity (PV) streamers or cut-off lows, and diabatic heating from deep convection (Galarneau et al., 2015; González-Alemán et al., 2015). This interplay gradually transforms the initial frontal structure into a symmetric, warm-core vortex, as the Hurricane Alex (2016) and Hurricane Ophelia (2017). A central feature of this transformation is the co-evolution of the primary and secondary circulations. As the primary circulation intensifies, an overturning secondary circulation emerges to facilitate the radial and vertical transport of heat, momentum, and mass (Peng et al., 2019).

Although the secondary circulation is fundamental to establishing thermal wind balance and sustaining intensification through planetary boundary layer (PBL) convergence (Montgomery and Smith, 2014), its specific role during TT process is not yet fully understood. Previous studies have used energy or PV frameworks to assess the balance between baroclinic and latent heat release, but these often lack the high-resolution, storm-centered detail necessary to isolate specific forcing mechanisms during the transition phase (Davis and Bosart, 2004; Galarneau et al., 2015; González-Alemán et al., 2015).Consequently, quantifying the vertical coupling and the shifting contributions of thermodynamic and momentum forcing in a TT process remains a significant challenge (Calvo-Sancho et al., 2022).

This study focuses on Hurricane Ophelia (2017) to increase the knowledge/understanding of these mesoscale mechanisms in a TT process. Hurricane Ophelia was a high-impact TT case in the northeastern Atlantic, which was the first TT to reach hurricane category 3 and caused notable socioeconomical impacts in Spain (extreme wildfires) and Ireland (extreme wind gusts and cyclonic storm surge; Guisado-Pintado and Jackson, 2019). This hurricane is selected from the TT database developed by Calvo-Sancho et al. (2022), which documents TT cases across the NATL based on a combination of dynamical and thermodynamical criteria. By employing high-resolution Weather Research and Forecasting (WRF) model simulations alongside energy budget and wind tendency diagnostics, we aim to explicitly isolate and quantify the mechanical drivers of the secondary circulation. This work represents the first high-resolution real-case study in a TT event to apply diagnostics previously reserved for idealized simulations and pure tropical hurricanes, providing new insights into the transition from baroclinic to diabatic dominance.

The work is organized as follows: Section 2 describes the numerical simulation configuration/setup and the diagnostic equations for the secondary circulation. Section 3 characterizes Ophelia's transition and interprets the evolution of its circulation through the applied diagnostics. Finally, Section 4 summarizes the findings and discusses their implications for future TT research.

2. Numerical simulation setup and secondary circulation

2.1. WRF setup

The TT Ophelia is simulated employing the high-resolution limited-area numerical weather prediction model Advanced Research WRF model (WRF-ARW), version 4.5 (Skamarock et al., 2019). The simulation starts on 09 OCT 2017 at 00:00 UTC and ends on 11 OCT 2017 at 18:00 UTC, covering the entire TT process and first hurricane intensification, allowing a 6 h spin-up, with a 5-min output.

The non-hydrostatic WRF-ARW model is configured with two domains with two-way nesting and centered on the TT (based on HURDAT data; (Landsea and Franklin, 2013). Each domain is 1000 x 1000 grid-points, with a horizontal resolution of 3 km for the outer domain (D01) and 1 km for the inner domain (D02). The vertical resolution is 65 sigma levels unequally spaced, with greater resolution in the lower troposphere to obtain a better representation of convective processes in the PBL. Adaptative time steps are used with the default WRF-ARW Hurricane research mode physics parametrizations, the most important being the WRF-ARW Single-Moment 6-class scheme for microphysics (Hong and Lim, 2006), the Yonsei University Scheme for the PBL (Hong et al., 2006) , the Dudhia Shortwave Scheme (Dudhia, 1989) and the RRTM Longwave Scheme (Mlawer et al., 1997) for radiation. Cumulus convection is explicitly computed by the model. Finally, the initial/boundary conditions are obtained from the Integrated Forecasting System (IFS) analysis model produced by the European Centre for Medium-Range Weather Forecast (ECMWF) with a 0.1° horizontal resolution, 6-h temporal resolution and 137 vertical model levels.

2.2. Secondary circulation

TCs are often conceptualized as quasi-axisymmetric systems that consist of a primary circulation (tangential wind) and a secondary circulation (radial-vertical flow), which is schematized in Fig. 1. In the balanced-vortex framework (Eliassen, 1951; Emanuel, 1986), the secondary circulation acts to ensure the maintenance of thermal wind balance. In this study, a detailed analysis of the secondary circulation (using the radial momentum and hydrostatic equations) and the potential temperature (θ) budget is conducted to better understand the internal processes occurring during the TT event analyzed.

The starting point for the analysis of the secondary circulation is the radial component of the momentum equation in a rotating frame, derived from the full vectorial form of the momentum equations in cylindrical coordinates. The general momentum equation is expressed as:

$$\frac{\partial \vec{v}}{\partial t} + (\vec{v} \cdot \nabla)\vec{v} + 2\Omega \times \vec{v} = -\frac{1}{\rho}\nabla p + \vec{g} + D_u,$$

where $\vec{v} = (u, v, w)$ is the wind vector in cylindrical coordinates, Ω is the Earth's rotation vector, ∇p the pressure gradient force, ρ the air density, $\vec{g}$ the acceleration due to gravity and D_u represents frictional and diffusive forces. The radial component of the momentum equation is

$$\frac{\partial u}{\partial t} = -u\frac{\partial u}{\partial r} - \frac{v}{r}\frac{\partial u}{\partial \phi} - w\frac{\partial u}{\partial z} + v\left(f + \frac{v}{r}\right) - c_p T\frac{\partial \ln \pi}{\partial r} + D_u, \tag{1}$$

where r is the radius, R the maximum radius, f the Coriolis parameter, u and v the radial and tangential wind components, respectively, and T the temperature. All dependent variables depend on (r, ϕ, z, t). The term π refers to the Exner function, defined as $\pi = \left(\frac{p}{p_0}\right)^{R_d/c_p}$, where R_d is the gas constant for dry air and c_p is the heat capacity of dry air at constant pressure. The Exner function relates θ to the actual temperature ($T = \pi\,\theta$) and plays a key role in the thermodynamic diagnostics.

Integrate Eq. (1) radially from $r = 0$ to $r = R$ along $z = 0$ to obtain:

$$\frac{\partial}{\partial t}\int_{r=0}^{r=R} u\Big|_{z=0} dr = -\int_{r=0}^{r=R}\left[\frac{v}{r}\frac{\partial u}{\partial \phi}\right]_{z=0} dr + \int_{r=0}^{r=R}\left[v\left(f + \frac{v}{r}\right) + D_u\right]_{z=0} dr + \; c_p T_s\left(\ln \pi|_{r=0,z=0} - \ln \pi|_{r=R,z=0}\right), \tag{2}$$

where T_s is the (constant) sea-surface temperature and $w|_{z=0} = 0$ and $u|_{r=0} = u|_{r=R} = 0$ are assumed. The first term on the right-hand side might be significant, but it will be ignored for now.

Then, integrate the hydrostatic equation ($c_p T\,\partial \ln \pi \,/\, \partial z = -g$) vertically:

$$\ln\ \pi|_{z=0} = \ln\ \pi|_{z=H} + \frac{g}{c_p}\int_{z=0}^{z=H}\frac{dz}{T} \tag{3}$$

and use Eq. (3) in Eq. (2) to obtain:

$$\frac{\partial}{\partial t}\int_{r=0}^{r=R} u\Big|_{z=0} dr = \int_{r=0}^{r=R}\left[v\left(f + \frac{v}{r}\right) + D_u\right]_{z=0} dr + c_p T_s\left[\ln\ \pi|_{\substack{r=0,\\ z=H}} - \ln\ \pi|_{\substack{r=R,\\ z=H}} + \frac{g}{c_p}\int_{z=0}^{z=H}\left(\frac{1}{T|_{r=0}} - \frac{1}{T|_{r=R}}\right) dz\right] \tag{4}$$

Along $z = H$, assume $u = v = 0$ and $D_u = 0$; the integral of (1) from $r = 0$ to $r = R$ at $z = H$ then gives

$$\ln\ \pi|_{r=0,z=H} = \ln\ \pi|_{r=R,z=H}, \tag{5}$$

so that Eq. (4) can be simplified to

$$\frac{\partial}{\partial t}\int_{r=0}^{r=R} u\Big|_{z=0} dr = \int_{r=0}^{r=R}\left[v\left(f + \frac{v}{r}\right) + D_u\right]_{z=0} dr + gT_s\int_{z=0}^{z=H}\left(\frac{1}{T|_{r=0}} - \frac{1}{T|_{r=R}}\right) dz. \tag{6}$$

Equation (6) expresses the time derivative of the secondary circulation (S) term, i.e. the secondary circulation $dS(t)/dt$, as a function of radially integrated centrifugal force + radial friction (first term on the right-hand side) and vertically integrated buoyancy force (second term on the right-hand side).

The last term in Eq. (6) can be simplified by letting

$$T|_{r=0} = T|_{r=R} + \tilde{T}, \tag{7}$$

here $\tilde{T}$ is a small perturbation of $T|_{r=R}$, i.e. $|\tilde{T}/T|_{r=R}| \ll 1$, which gives

$$\frac{dS(t)}{dt} = -\frac{\partial}{\partial t}\int_{r=0}^{r=R} u\Big|_{z=0} dr = gT_s\int_{z=0}^{z=H}\frac{\tilde{T}(0,z)}{T^2|_{r=R}} dz - \int_{r=0}^{r=R}\left[v\left(f + \frac{v}{r}\right) + D_u\right]_{z=0} dr. \tag{8}$$

For $\int_{z=0}^{z=H} \frac{\tilde{T}(0,z)}{T^2|_{r=R}} dz > 0$, the secondary circulation Eq (8) represents the thermal tendency to produce an "in-up-out" circulation and the opposing effect of centrifugal and frictional forces.

The final step is to integrate over ϕ from 0 to 2π which will be denoted as $\langle \dots \rangle = \int_0^{2\pi} (\dots) d\phi$. The final equation (now including $(v/r)\,\partial/\partial\phi$) is:

$$\frac{\partial}{\partial t}\int_{r=0}^{r=R} \langle -u|_{z=0}\rangle dr = \int_{r=0}^{r=R} \left\langle \frac{v}{r}\frac{\partial u}{\partial \phi}\right\rangle_{z=0} dr - \int_{r=0}^{r=R} \left\langle v\left(f+\frac{v}{r}\right)+D_u\right\rangle_{z=0} dr + gT_s\left\langle \int_{z=0}^{z=H} \frac{\tilde{T}}{T^2|_{r=R}} dz\right\rangle \tag{9}$$

It is important to note that (u, v) is computed as

$(u, v) = (u_c \cos\phi + v_c \sin\phi, v_c \cos\phi - u_c \sin\phi)$

from the Cartesian components (u_c, v_c). The azimuthal integral is done only for the last Eq. (9), which matters since $\langle v^2\rangle \neq \langle v\rangle^2$.

To simplify the interpretation of the buoyancy term, it is useful to introduce θ which is adiabatically conserved and related to T through the approximation

$$\frac{\tilde{T}}{T|_{r=R}} \approx \frac{\tilde{\theta}}{\theta|_{r=R}}$$

The θ budget (Eq. (10)) is computed following four steps.

$$\frac{\partial\tilde{\theta}}{\partial t} = -\frac{1}{r}\frac{\partial}{\partial r}(ru\tilde{\theta}) - \frac{1}{r}\frac{\partial}{\partial \phi}(v\tilde{\theta}) - \frac{\partial}{\partial z}(w\tilde{\theta}) + Q, \tag{10}$$

where $\tilde{\theta} = \theta - \theta|_{r=R}$, $\theta|_{r=R}$ is assumed constant and Q is the diabatic heating.

- Step 1: Compute the azimuthal average

$$\langle(\dots)\rangle = \frac{1}{2\pi}\int_0^{2\pi} (\dots) d\phi$$

of Eq. (10) to obtain

$$\frac{\partial\langle\tilde{\theta}\rangle}{\partial t} = -\frac{1}{r}\frac{\partial}{\partial r}\left(r\langle u\tilde{\theta}\rangle\right) - \frac{\partial}{\partial z}\left(\langle w\tilde{\theta}\rangle\right) + \langle Q\rangle \tag{11}$$

- Step 2: Compute volume average for $0 \le r \le r_e$ and $0 \le z \le H$, defined as:

$$\hat{\theta} = \frac{1}{\pi r_e^2 H}\int_0^{r_e}\int_0^{H}\int_0^{2\pi} \tilde{\theta}\, r d\phi dr dz = \frac{2}{r_e^2 H}\int_0^{r_e}\int_0^{H}\left(\int_0^{2\pi}\tilde{\theta}\, d\phi\right) r dr dz = \frac{2}{r_e^2 H}\int_0^{r_e}\int_0^{H}\langle\tilde{\theta}\rangle\, r dr dz, \tag{12}$$

where r_e is the eyewall radius and H the system height.

Apply Eq. (12) to Eq. (11):

$$\frac{\partial\hat{\theta}}{\partial t} = -\frac{2}{r_e H}\int_0^{H} \langle u\tilde{\theta}\rangle_{r=r_e} dz + \hat{Q} \tag{13}$$

- Step 3: Decomposition, let

$$u(r,\phi,z) = \langle u\rangle + u'(r,\phi,z) \tag{14}$$

and

$$\tilde{\theta}(r,\phi,z) = \langle\tilde{\theta}\rangle + \tilde{\theta}'(r,\phi,z), \tag{15}$$

so that

$$\langle u\tilde{\theta}\rangle = \langle u\rangle\langle\tilde{\theta}\rangle + \langle u'\tilde{\theta}'\rangle + O^2. \tag{16}$$

- Step 4: Substitute Eq. (16) into Eq. (13)

$$\frac{\partial\hat{\theta}}{\partial t} = -\frac{2}{r_e H}\int_0^H \left(\langle u\rangle\langle\tilde{\theta}\rangle + \langle u'\tilde{\theta}'\rangle\right)_{r=r_e} dz + \hat{Q} \tag{17}$$

The two terms in the integral represent the mean and the eddy heat flux into the cylinder, respectively ($0 \leq r \leq r_e; 0 \leq z \leq H$; Fig. 1).

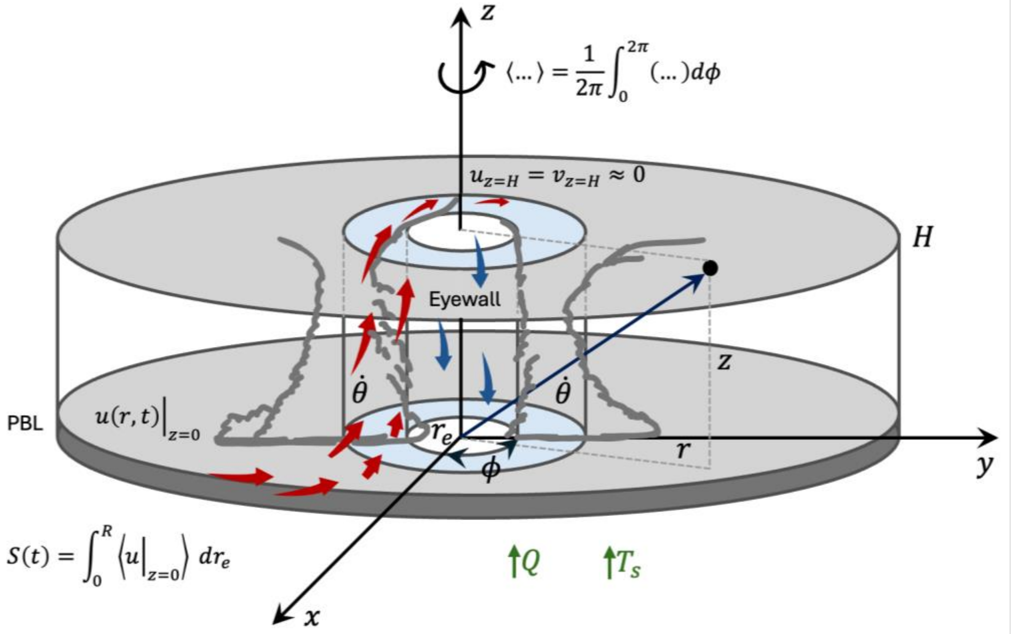

Figure 1: Schematic of the secondary circulation $S(t)$ in cylindrical coordinates, showing surface inflow, eyewall ascent, and upper-level outflow (red arrows). Blue arrows indicate subsidence. Key variables, circulation and azimuthal mean are shown. Green arrows denote mixing ratio and surface fluxes.

While Eq. (17) serves as the mathematical basis for deriving the volume-integrated θ budget, aiming to separate mean and eddy heat fluxes entering the cyclone's inner core, a different diagnostic approach is required to examine the vertical structure of the warming. To this end, Eq. (18) is employed to analyse the vertical profile of θ tendencies specifically at the cyclone centre (Peng et al., 2019). Unlike Eq. (17), this advective formulation allows for the direct quantification of the specific physical processes, such as microphysics versus vertical advection, that are responsible for the heating or cooling observed at different altitudes.

$$\frac{\partial \theta}{\partial t} = -u\frac{\partial \theta}{\partial r} - w\frac{\partial \theta}{\partial z} + \dot{q} + D_\theta + R + N_\theta, \tag{18}$$

where $\dot{q}$ is the tendency from the microphysical scheme, D_θ the turbulence tendency, R the tendency from radiation term and N_θ the tendency from Rayleigh damping (Bryan and Rotunno, 2009).

3. Results

3.1. System characterization

3.1.1. Synoptic and satellite evolution

Analyzing the synoptic-scale evolution that led to the TT of Ophelia is fundamental to understanding how it transitioned from an initially non-tropical system into a fully developed TC. Figure 2a illustrates the presence of a cut-off low at 300 hPa in the NATL (≈ 30ºN, 40ºW), which acts as a catalyst for surface cyclogenesis (Calvo-Sancho et al., 2022; González-Alemán et al., 2015). This cut-off low represents the dominant synoptic feature prior to the TT, providing the necessary dynamic support for cyclogenesis. One of the main characteristics of TT events is the presence of a robust anticyclone situated to the north-northeast of the surface cyclone (Galarneau et al., 2015). However, in the case of Ophelia, as depicted in Figs. 2a-c, this anticyclone is positioned slightly northwest of the developing cyclone. The role of the anticyclone is crucial as it facilitates moisture advection into the system. This process is reinforced by enhanced surface latent heat fluxes, which are intensified in regions with a strong pressure gradient associated with large surface winds. The resulting moisture convergence helps with the deep convection required for the transition to a warm-core system. As time progresses, the cut-off low undergoes significant evolution, leading to an increase in geopotential at 300 hPa (Z300; Figs. 2b, c). This increase is indicative of a warm-core transition (Calvo-Sancho et al., 2022), marking a fundamental shift in the cyclone's structure from an initial baroclinic system to a more tropical-like state, as it reduces baroclinicity and enhances symmetric convection around the cyclone centre, ultimately favoring TC formation.

The evolution of the cut-off low not only influences the synoptic structure preceding the TT but also facilitates the intrusion of PV streamers into lower latitudes. These PV filaments are often associated with upper-tropospheric troughs (Sadler, 1967; Wernli and Sprenger, 2007), which are dynamically active regions associated with anticyclonic wave breaking (Thorncroft et al., 1993) and can contribute to the formation of cut-off lows. These PV streamers extend southwestward, facilitating the intrusion of cyclonic PV into lower latitudes and enhancing the likelihood of TT events. As the cut-off low evolves, the moisture advection driven by the surrounding anticyclone, combined with the reduction in baroclinicity, favors the system's symmetrisation and the development of a warm-core structure in the mid-to-upper levels, as seen in Fig. 2. The introduction of a differential diabatic heat source within the air column causes a redistribution of PV through diabatic heating (Cammas et al., 1994; Hulme and Martin, 2009). As noted by (Hoskins et al., 1985), PV is largely conserved along parcel trajectories in a Lagrangian framework when advection dominates over diabatic and frictional influences. During the early stages of TT, significant latent heat release, particularly in the lower troposphere, enhances PV locally. This intensification, as shown by

https://doi.org/10.5194/egusphere-2026-1446
Preprint. Discussion started: 30 March 2026

Hulme and Martin (2009) and Calvo-Sancho et al. (2022), leads to the concentration of high PV regions near the cyclone centre, strengthening the system's circulation. Concurrently, as TT advances, upper-tropospheric PV decreases. This contrasting behavior between upper and lower PV distribution is attributed to non-advective PV tendencies (Cammas et al., 1994; Hulme and Martin, 2009). This pattern is evident in Figs. 2d-f, which illustrate average PV at 300–200 hPa from $t_0 - 24h$ to $t_0 + 24h$ (being t_0 the TT time), clearly depicting a PV streamer intrusion into lower latitudes before Ophelia's TT (Fig. 2d). This behavior aligns with the evolution of the Z300 in Figs. 2a-c, where Rossby wave breaking is appreciated. As TT progresses, a decrease in the Averaged Potential Vorticity (APV) at 300–200 hPa (Fig.2 e, f) and an increase at 900–800 hPa (Figs. 2g-i) can be appreciated around the cyclone centre (≈ 30ºN, 40ºW), which is consistent with findings from Calvo-Sancho et al., 2022), among other studies.

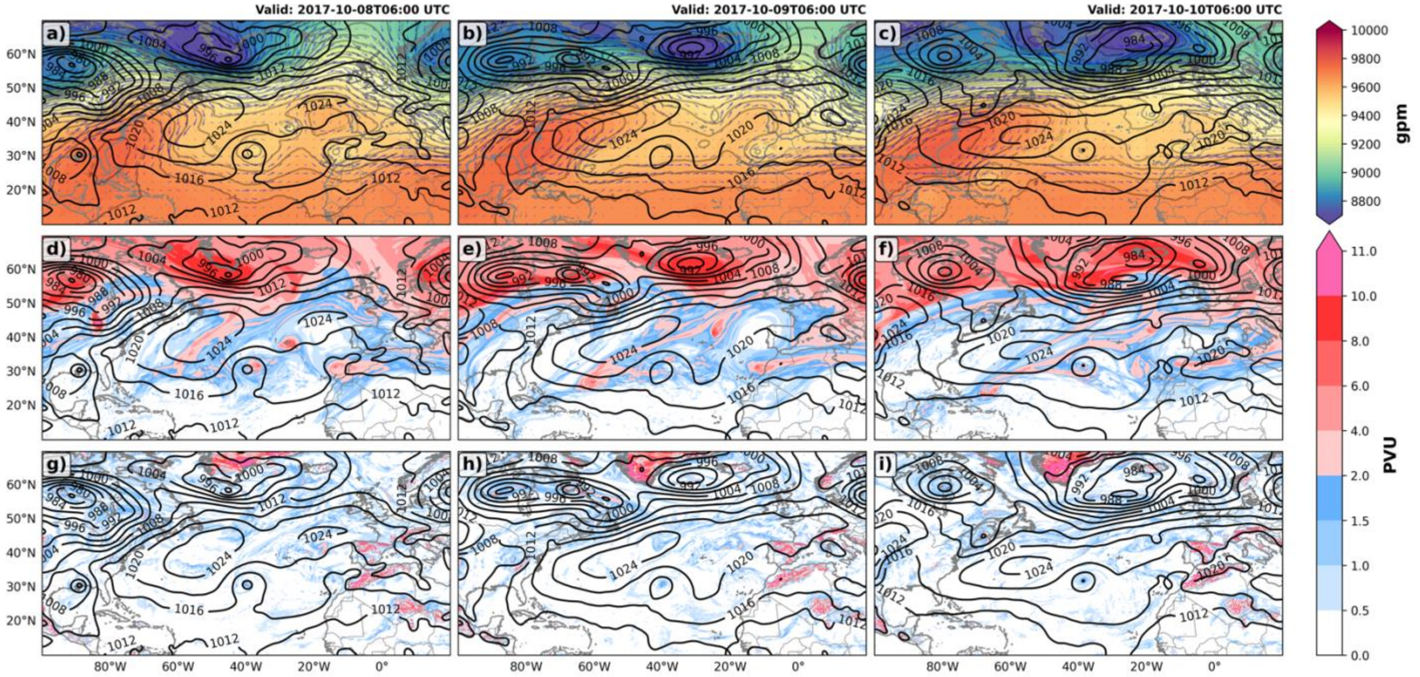

Figure 2: Z300 (gpm) a) at $t_0 - 24h$; b) at t_0; and c) at $t_0 + 24h$. APV (PVU) in the upper-troposphere (200-300 hPa) d) at $t_0 - 24h$; e) at t_0; and f) at $t_0 + 24h$. APV (PVU) in the lower-troposphere (850-925 hPa) g) at $t_0 - 24h$; h) at t_0; and i) at $t_0 + 24h$. Black contours depict the Mean Sea Level Pressure (MSLP; hPa).

To continue, the brightness temperature from the SEVIRI (IR10.8) satellite is analyzed for the Ophelia's TT. In Fig. 3a, where the dominant perturbation energy source is a consequence of baroclinic instability, the system is not organized and presents scattered convection. There is no clear small-scale central circulation, and convective bursts are irregularly distributed. Moreover, cloud tops are not particularly cold, indicating shallow convection. In contrast, convection becomes more concentrated in Fig. 3b, and a well-organized system can be seen. Now, the system begins to lose its baroclinic structure and gradually starts drawing energy from latent heat release. The presence of persistent deep convection near the centre suggests the development of a warm core. Finally, a well-defined, symmetric annular ring cloud structure is evident in Fig. 3c. The cloud band within this ring has led to subsidence in its interior (Smith and Montgomery, 2016), as indicated by the lack of deep convection at the cyclone's centre. Convection is now organized around the system's core, suggesting the development of a mature warm-core structure. This confirms that the system has fully transitioned into a TC.

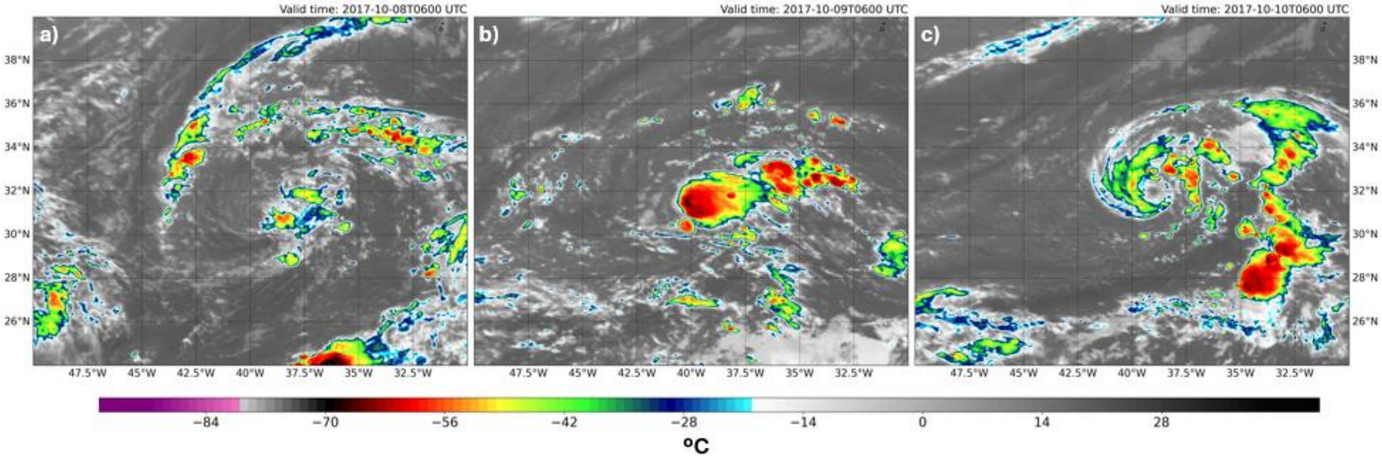

Figure 3: SEVIRI channel 9 brightness temperature (°C) a) at $t_0 - 24h$; b) at t_0; and c) at $t_0 + 24h$.

3.1.2. WRF-ARW solution

To provide a temporal framework for the diagnostic analysis presented hereafter, Fig. 4 illustrates the evolution of the fundamental intensity and structural metrics of Hurricane Ophelia. These time series are essential for delineating the TT period (indicated by the gray shaded area), distinguishing the initial baroclinic phase from the subsequent mature TC stage. The minimum Mean Sea Level Pressure (MSLP) time series in Fig. 4 depicts a two-phase intensification in Hurricane Ophelia: the TT period (Figs. 4a, b; gray shaded) and afterwards. The black line shows minimum MSLP related to short-term fluctuations, likely associated with stronger convective pulses typical of TT periods and TC eyewalls. These fluctuations are indicative of transient local updraft maxima and dynamic eyewall replacement cycles (Davis and Bosart, 2003; Kossin and Sitkowski, 2009). In contrast, the blue line displays the larger-scale minimum MSLP, after applying an eight-step Gaussian filter, showing the persistent influence of secondary circulations mechanisms (such as organized ascent within the cyclone core and compensating subsidence at the outer radius), which are crucial to maintaining storm intensity. The MSLP remains quasi-steady during the first 15 h of 9 October, consistent with the presence of a baroclinic, cold-core cyclone (Fig. 4a). This initial period gives way to a transition period marked by a rapid pressure drop of approximately 6 hPa over 12 h. This pressure drop coincides with the emergence of stronger mesoscale convective bursts, consistent with the *hot towers* concept described by Montgomery and Smith (2014). These convective structures enhance diabatic heating and radial inflow, thereby intensifying the system's secondary circulation and leading to a hydrostatic reduction in MSLP. After the TT period, a pronounced pressure drop occurs within 24 h (from ≈ 1003 to ≈ 975 hPa). This rapid MSLP deepening may be associated with the positive SST anomaly in the central and eastern NATL (not shown), which enhances latent and sensible heat fluxes from the ocean surface and thus supports the maintenance and intensification of TCs (Davis and Bosart, 2004; Emanuel, 1986).

Figure 4b shows the evolution of the maximum tangential velocity (V_m) and the radius of maximum wind speed (RMW). Initially, the cyclone exhibits modest V_m with a very noisy RMW during the first 14h, characteristic of a baroclinic, hybrid cyclone or a weakly organized tropical disturbance (Montgomery and Smith, 2014). The maximum tangential wind V_m begins to increase markedly at the time the TT phase starts, which is related to convection bursts (Fig. 3b) (Peng et al., 2019). During the TT phase, the RMW initially decreases significantly to around 12 km, then undergoes oscillations before reaching up to 40–45 km. Finally, it contracts further to approximately 20 km in the final stage of the TT, reflecting a transition marked by core tightening and cyclone intensification. This evolution is typical in early intensifying stages in TCs or ending TT phase (Willoughby et al, 1982; Stern and Nolan, 2011). After the TT ends, V_m continues increasing accompanied by a sustained RMW. This continued intensification indicates stability of the inner core despite a moderate shear environment, which results in the maintenance of secondary circulation (Davis and Bosart, 2003; Smith and Montgomery, 2015).

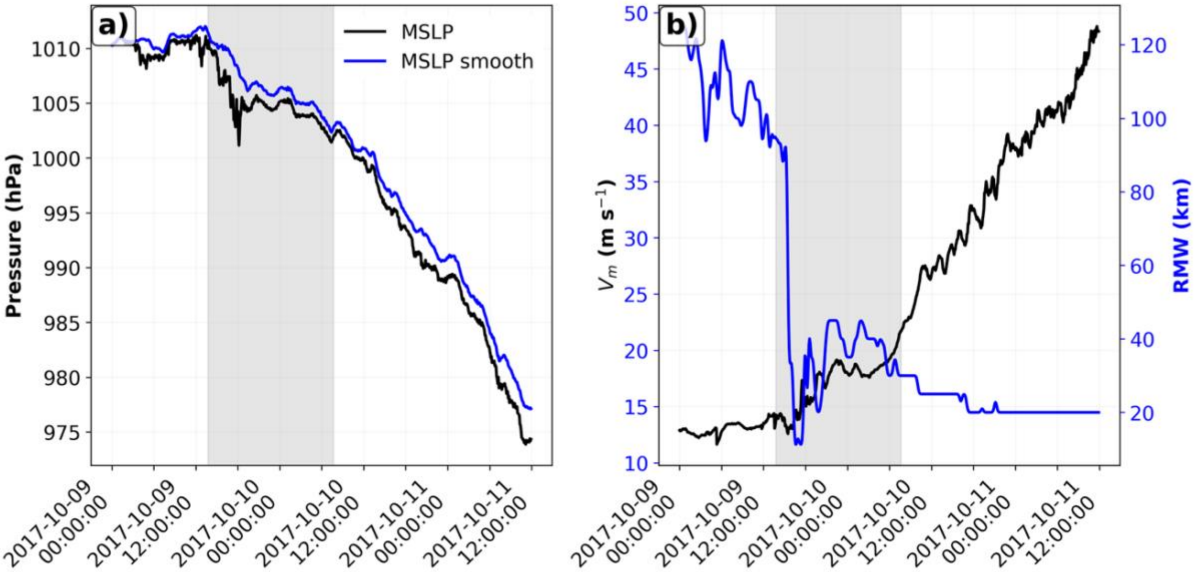

Figure 4: Time-series of a) minimum MSLP (black; hPa) and smoothed MSLP (hPa) applying a Gaussian filter (blue); b) V_m (left axis; black; m s^{-1}) and the RMW (right axis; blue; km). The gray bar denotes the TT period.

Figure 5 shows the WRF-ARW solution before, during and after the TT of Hurricane Ophelia from the point of view of the Outgoing Longwave Radiation (OLR) and equivalent potential temperature (θ_e) west-to-east cross-section centered in the minimum sea level pressure in each timestep. Prior to the TT, the OLR shows a mesoscale convective system at the northeastern surface cyclone centre (Fig. 5a), where the baroclinic structure of the system dominates due to the cold core, as depicted by the θ_e cross-section in Fig. 5b. Figure 5c shows the initiation of convection organized around the surface centre,

https://doi.org/10.5194/egusphere-2026-1446
Preprint. Discussion started: 30 March 2026

which is characteristic of diabatic processes due to the convection that takes place and redistributes the PV (Fig. 2b). As a result, Fig. 5d illustrates how the cyclone centre begins to warm progressively, demonstrating enhanced secondary circulation due to strong input of high θ_e in low levels and large diabatic heating near the eyewall region (Emanuel, 1986). The transition process involves complex interactions between baroclinic forcing and deep convection, whereby diabatic heating increasingly dominates the cyclone energetics and structural evolution (Davis, 2010; Evans and Hart, 2003).

Finally, the early stage of a TC formed through TT typically exhibits a compact warm-core structure, characterized by a notably small eyewall radius (around 20 km; Figs. 5e, f) and comparatively weaker peak wind gusts than those observed in cyclones originating from easterly wave disturbances (Davis and Bosart, 2004; Hart et al., 2006). During this transitional phase, the cyclone retains certain baroclinic characteristics due to high-level cloud formations in the southwestern quadrant (Fig. 5e), indicative of ongoing asymmetric dynamics influenced by moderate vertical wind shear (Jones et al., 2003). At this stage, the diabatic processes dominate and the cyclone achieves a clear warm-core vertical structure, evident in the thermal anomaly (Fig. 5f; Montgomery and Farrell, 1993; Emanuel, 1995).

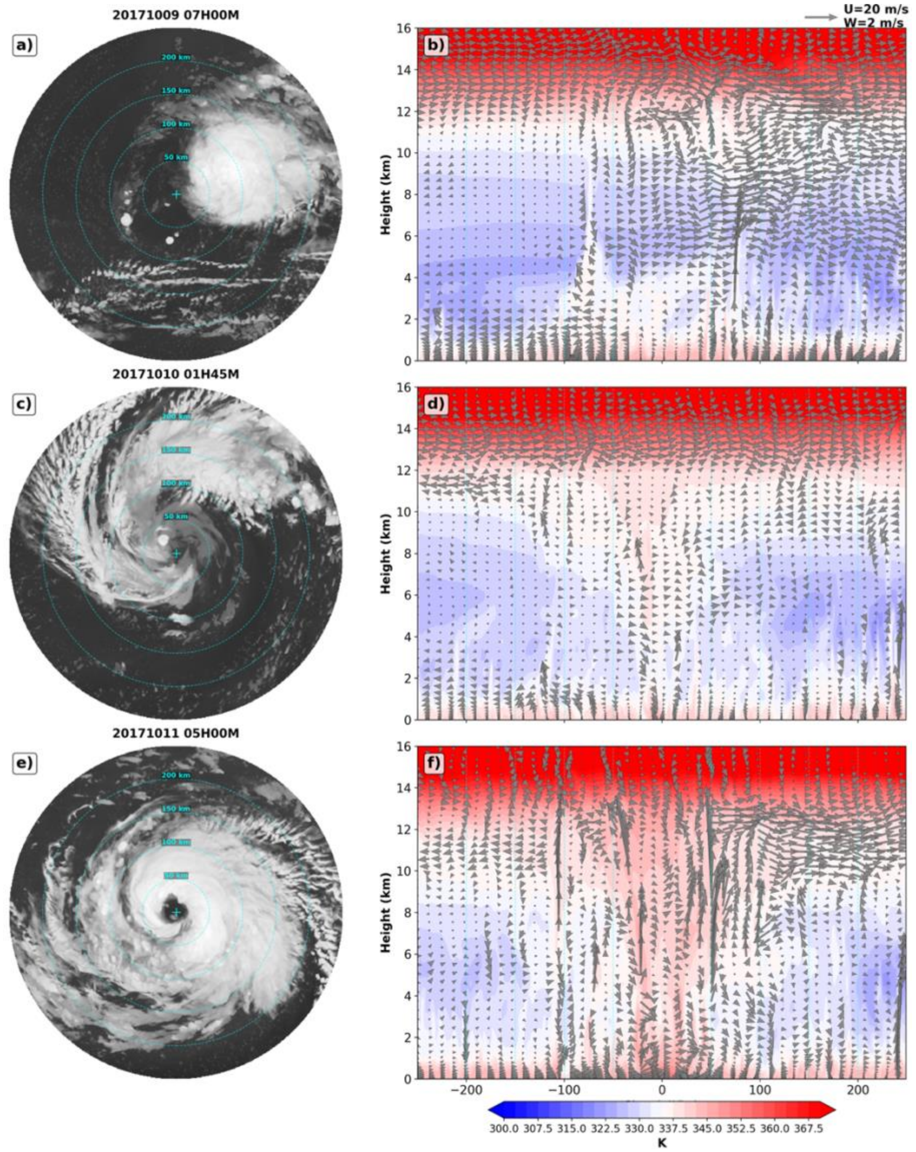

Figure 5: a) OLR imagery and b) θ_e cross-section (K) centered in the minimum MSLP from the WRF-ARW simulation before the TT (2017-10-09 07:00 UTC). c) OLR imagery and d) θ_e cross-section (K) centered in the minimum SLP from the WRF-ARW simulation during the TT (2017-10-10 01:45 UTC). e) OLR imagery and f) θ_e cross-section (K) centered in the minimum MSLP from the WRF -ARW simulation after the TT (2017-10-11 05:00 UTC). Blue cross in OLR imagery (a, c, e) indicates the cyclones' centre. Vectors in the cross-section (b, d, f) denote the vertical and zonal wind.

3.2. Secondary circulation

Figure 6a shows the fundamental components governing the circulation tendency specified in Eq. (9), breaking it down into three key terms: the centrifugal/Coriolis, the thermal and the frictional term. Note that the centrifugal force gives $\mathrm{dS/dt} > 0$ and buoyancy gives $\mathrm{dS/dt} < 0$; thus, the thermal term is plotted with a negative sign to ease comparison. Before TT begins, all contributions remain nearly constant. However, as soon as TT starts (indicated by the gray bar), thermal and centrifugal terms begin increasing at nearly the same rate. This suggests that, during the transition phase, the centrifugal and thermal forcings are nearly balanced. The frictional term remains nearly constant for the entire period, except for a slight increase at the beginning of the TT, which is the signature of initial convective bursts (Davis and Bosart, 2004). Once the cyclone has fully transitioned, thermal forcing overcomes the opposing centrifugal tendency indicating it intensifies the secondary circulation and thus the entire system (Bosart and Lackmann, 1995; Emanuel, 1986).

In Fig. 6b, the circulation term S(t) is shown. Before the transition begins, S(t) does not exhibit a clear increasing tendency, which indicates that the baroclinic forcing dominates the system evolution. However, as the TT begins, S(t) starts to increase sharply, which is in line with the simultaneous rise in the thermal forcing and the opposing centrifugal force in Fig. 6a. It should be noted that after the initial peak of the gray area (TT period), there is a temporary decrease before the circulation resumes its upward trend after TT, which can be related to a brief decrease in secondary circulation strength due to structural adjustment, as the system momentarily loses baroclinic support before fully relying on convective processes (Quitián-Hernández et al., 2020). As mentioned, when the TT is completed, the cyclone intensifies through latent heat release from deep convection, leading to the intensification of the eyewall ascending motions, which strengthens the S(t).

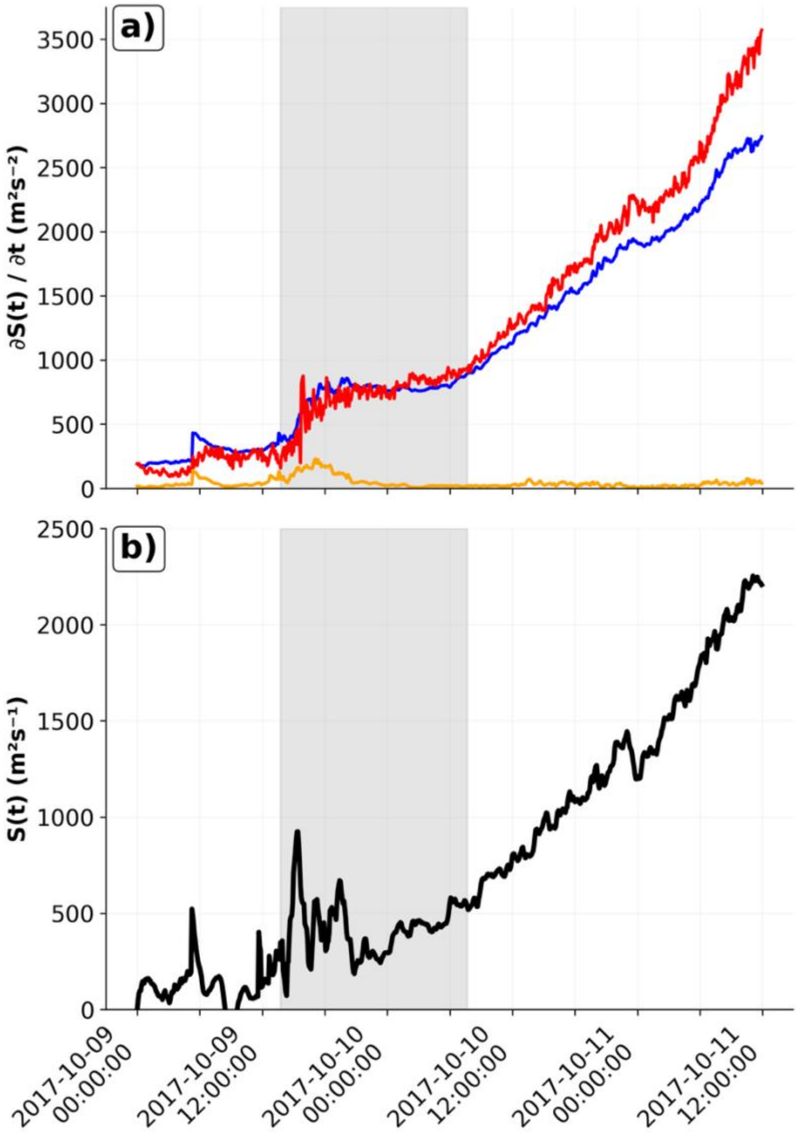

Figure 6: a) Time evolution of the negative of the centrifugal term (blue); the thermal term (red); and the frictional term (yellow) of $\frac{\partial S(t)}{\partial t}$ (m^2s^{-2}). b) Time evolution of $S(t)$ (m^2s^{-1}). The gray bar denotes the TT period.

To trace the thermodynamic origin of the buoyancy dominance established above, the thermodynamic evolution of the cyclone as it undergoes TT is illustrated in Fig. 7, tracking the relationship between the maximum θ_e at three distinct vertical levels (z = 0, 2500, 5000 m) and the maximum θ at the cyclone centre (r = 0). During the early stages of the transition (represented by cooler colors) there is little to no substantial heating observed (Figs. 7a-c), suggesting that the thermodynamic transformation is not yet underway at that point. However, it is important to note that during this initial phase, the maximum θ_e decreases with

https://doi.org/10.5194/egusphere-2026-1446
Preprint. Discussion started: 30 March 2026

height, indicating a cooler thermal structure aloft. Specifically, the minimum values are approximately 339 K at the surface (Fig. 7a), around 333 K at mid-levels (Fig. 7b), and near 327 K at upper levels (Fig. 7c).

At the cyclone centre (r = 0), the maximum θ value reaches almost 352 K by the final timestep, aligning with the system's complete transformation into a TC. It should be noted that this peak value slightly decreases to around 350 K toward the final timesteps. The warming is most pronounced near the surface, as shown in Fig. 7a, where the peak maximum θ_e at z = 0 reaches about 355 K before the end of the simulation period. In contrast, Figs. 7b and c reveal that at mid (z = 2500 m) and upper (z = 5000 m) levels, respectively, the maximum θ_e remains nearly constant once the θ_e of approximately 344 K is reached. These maximum values are achieved during the final stages of the transition, indicating a delayed thermodynamic response at higher altitudes relative to the near-surface layer. This behavior is consistent with the theoretical framework of TC maintenance (Emanuel, 1986; Hulme and Martin, 2009): the progressive θ_e increase at z = 0 m and the central core θ demonstrate that the structural evolution is driven principally by diabatic heat release derived from surface moisture fluxes (Rotunno and Emanuel, 1987). However, the core θ continues to rise at upper levels (Figs. 7b, c) even after the local θ_e stabilizes, which highlights the role of deep convection. The upper-tropospheric warming is not determined by local properties but is actively maintained by the continuous vertical transport of high energy air from the surface. This vertical structure highlights that the most intense warming, and thus the most tropical-like thermodynamic characteristics, emerge first at lower levels and then propagate upward as the cyclone transitions into a fully tropical system.

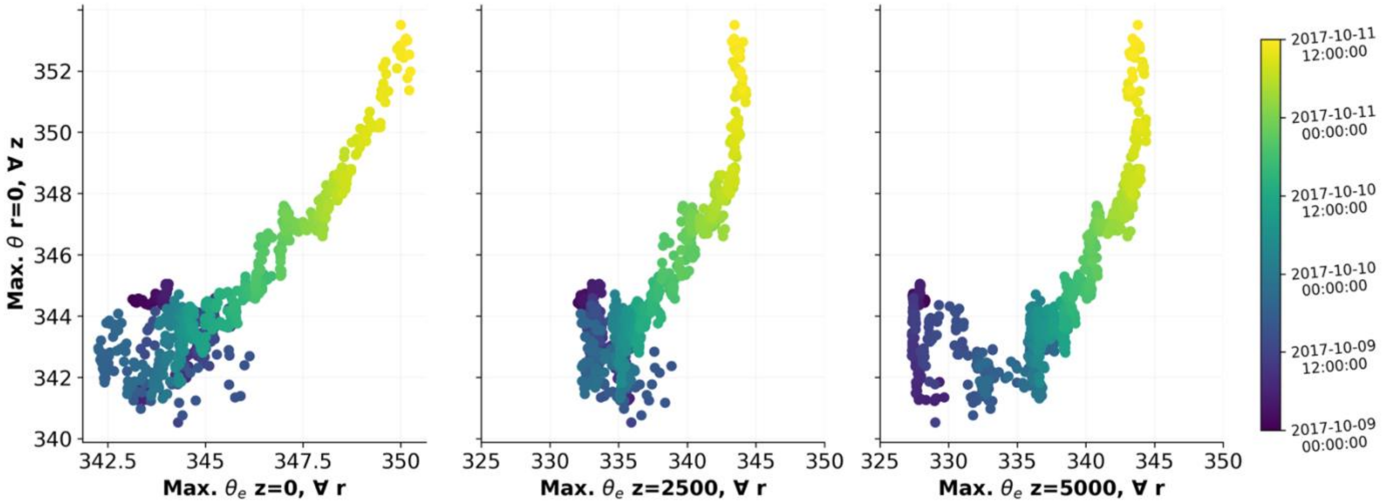

Figure 7: Time evolution (five-min time step) of the maximum θ (K) in the cyclone centre (r = 0 m) ∀z against the maximum θ_e (K) at a) z = 0 m; b) z = 2500 m; and c) z = 5000 m ∀r.

Given the critical role of the θ_e near the surface in driving the TT, the time-averaged θ_e budget for the 1000 – 925 hPa vertical layer is analyzed for the TT period (Fig. 8a; gray shaded in Fig. 6) and the post-TT period (Fig. 8b). This separation allows the relative contributions of the individual budget terms (Rotunno and Emanuel, 1987; section 4b) to be clearly identified during each stage of development. Following Rotunno and Emanuel (1987), the budget is evaluated over the radial interval from r = 0 to r = 250 km, ensuring that the PBL θ_e structure is adequately resolved and accurately represented. Previous work by Emanuel (1986) demonstrated that θ_e behavior in TCs is effectively characterized by subdividing the domain into the eye, the eyewall, and the outer region. This framework provides a useful basis for interpreting the radial variations in the θ_e budget and for diagnosing the dominant thermodynamic processes operating within each region.

The time-averaged θ_e budget ($\frac{\partial\theta_e}{\partial t}$; Figs. 8a, b) is decomposed into four primary contributions (Rotunno and Emanuel, 1987): mean θ_e radial advection $\left(-u\frac{\partial\theta_e}{\partial r}\right)$, mean θ_e vertical advection $\left(-w\frac{\partial\theta_e}{\partial z}\right)$, radial θ_e diffusion $\left(-\frac{1}{r}\frac{\partial rF_r^{\theta_e}}{\partial r}\right)$, and vertical θ_e diffusion$\left(-\frac{\partial F_z^{\theta_e}}{\partial z}\right)$. Additionally, the contribution from radiative processes is included (R). In both phases, a numerical residual is observed since the total θ_e tendency does not perfectly coincide with the sum of the individual physical components. Notably, Fig. 8a (TT phase) presents a larger residual magnitude than Fig. 8b, which is consistent with the presence of strong gradients that require increased implicit smoothing by the model (Zhang et al., 2000). As discussed by Calvo-Sancho *et al.* (2023a) regarding energy budgets, defining terms via residuals captures not only physical processes but also the model's numerical dissipation and boundary-condition effects.

It is appreciated that Fig. 8a presents lower intensities than Fig. 8b. During the TT phase (Fig. 8a), vertical diffusion is the dominant source of θ_e, while the advection terms have not yet reached their peak amplitudes, indicating that the secondary circulation is still intensifying. Vertical diffusion and vertical advection both contribute positively, reaching their maximum values within the eyewall region, consistent with the location of strongest upward motion. Beyond r ≈ 50 km, these contributions gradually decrease, with vertical advection diminishing more rapidly. In contrast, radial advection contributes negatively within the eyewall, reaching a minimum of approximately − 0.4 K h^{-1}. Farther outward, a weak and non-significant positive contribution appears near r ≈ 60 km. Radial diffusion and radiative processes play a negligible role throughout, with values oscillating around 0 K h^{-1}. Vertical diffusion being the primary source reflects the air-sea interaction. It represents the convergence of turbulent vertical fluxes. During this phase, the ocean acts as a more important source of energy for the PBL than the still-weak redistribution of energy by the secondary circulation. In addition, positive contribution from the vertical advection indicates that organized updrafts are beginning to transport air from the surface into upper levels. The peak in the eyewall indicates where the convection is concentrated. Finally, the negative contribution of radial advection in the eyewall represents the import of lower-entropy environmental air into the developing core, which reduces the storm's thermodynamic efficiency (Rotunno and Emanuel, 1987) and acts as a barrier to rapid intensification (Tang and Emanuel, 2012).

Figure 8b clearly depicts a later cyclone phase in which the secondary circulation has become more prominent. The cyclone exhibits a more organized structure, as indicated by the higher (relative to Fig. 8a) peaks of all budget terms, which are tightly confined to the eyewall and rapidly decay toward zero in the outer regions. In this phase, vertical advection dominates over vertical diffusion, in contrast to the behavior observed in Fig. 8a. Indeed, the larger magnitudes over the eyewall compared to the TT phase indicate that the secondary circulation is nearly fully developed, acting as the primary mechanism that redistributes energy acquired at the surface throughout the upper levels. The dominance of vertical advection in the eyewall

https://doi.org/10.5194/egusphere-2026-1446
Preprint. Discussion started: 30 March 2026

region suggests that deep convection has become the leading process for upward energy transport. Additionally, the large negative contribution from radial advection can be linked to anan intensified “ventilation” of the cyclone core, a characteristic feature of mature TCs (Emanuel, 1986; López-Reyes et al., 2025; Rotunno and Emanuel, 1987). The enhanced vertical advection and diffusion terms relative to the TT phase, together with the stronger negative radial advection, indicate that the system has reached a quasi-steady state, in which the total θ_e tendency remains close to zero as surface heating is balanced by energy transport and cooling associated with the secondary circulation.

Following Rotunno and Emanuel (1987), the θ_e budget in the PBL is decomposed into moist and dry components to clarify the processes controlling entropy variability during the cyclone evolution (Figs. A1, A2). During the TT phase (Fig. A1), the total θ_e tendency reflects a near balance between moist and dry contributions, consistent with a still-organizing system, although moist processes already dominate radial and vertical advection in the eyewall, indicating the early importance of moisture-rich inflow and upward transport. Radial diffusion shows comparable moist and dry contributions, while vertical diffusion is strongly moist dominated, highlighting the key role of surface moisture fluxes even at this stage. In the post-TT period (Fig. A2), the overall partitioning remains similar, but the amplitudes increase as the vortex intensifies and coupling between the ocean, PBL, and deep convection strengthens. Moist contributions become increasingly dominant near the cyclone centre and in the eyewall, reflecting stronger surface winds, enhanced enthalpy fluxes, and more efficient convective transport. A distinctive feature of this mature stage is a localized reduction in the moist contribution over the eyewall, attributable to intense PBL mixing and convective venting, where downward mixing of relatively drier air and strong updrafts can offset surface evaporation, highlighting the competition between surface-driven moistening and convective export.

https://doi.org/10.5194/egusphere-2026-1446
Preprint. Discussion started: 30 March 2026

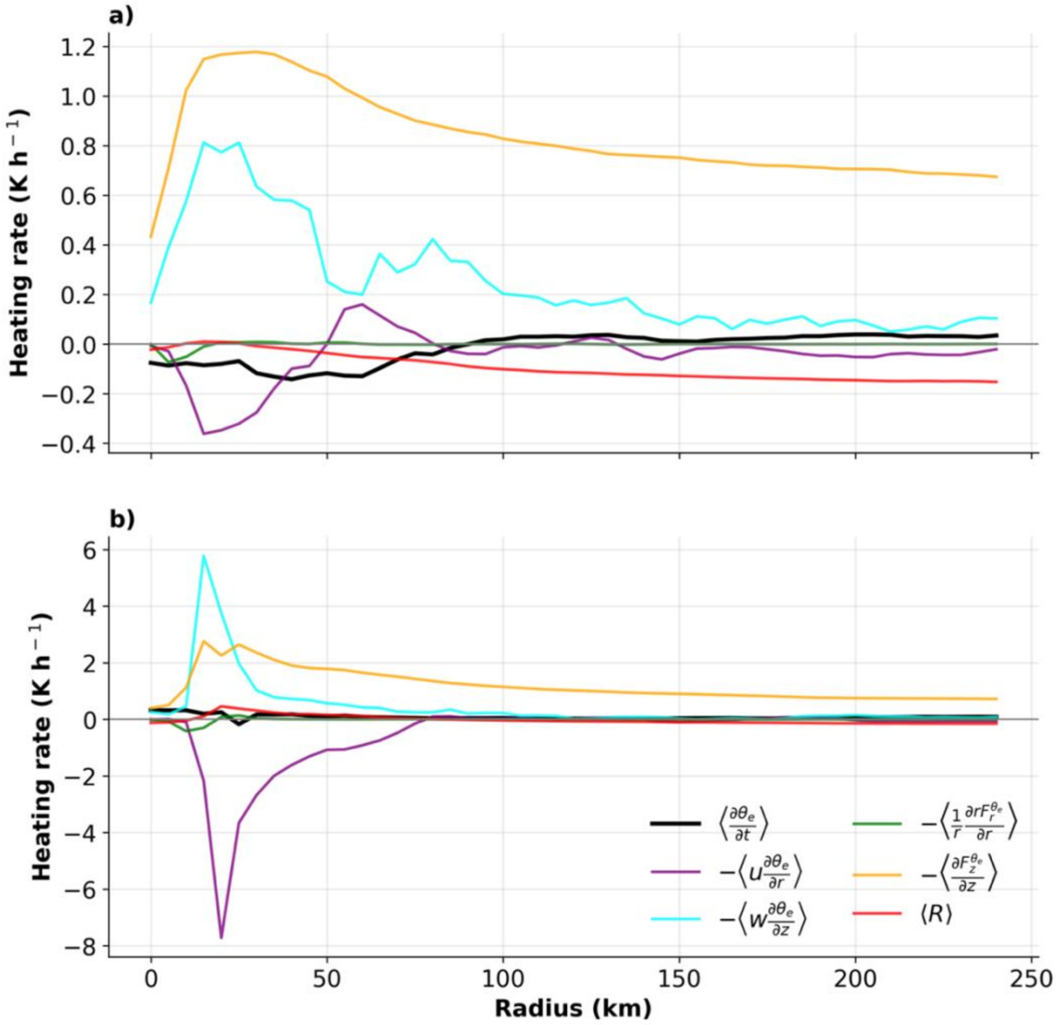

Figure 8: Time-averaged azimuthal mean of the θ_e budget (black); mean θ_e radial advection (purple), mean θ_e vertical advection (blue), radial θ_e diffusion (green), vertical θ_e diffusion (yellow) and radiative processes (red) for the 1000 – 925 hPa vertical layer during the a) TT period (gray shaded in Fig. 6) and the b) post-TT period. Terms derived following Rotunno and Emanuel (1987).

While the Fig. 8 analyses confirmed the surface-driven nature of the warm core, it presents a static view that masks the temporal intermittency of the processes. To quantify the dynamic influence of individual convective episodes versus the steady secondary circulation, Fig. 9 tracks the time evolution of the volume-integrated θ budget terms derived in Eq. (17). By monitoring these terms throughout the event, we can identify specific episodes where structural reorganization occurs driven by convective pulses. Initially, from October 9 through early October 10, the θ tendency remains close to zero, indicating minimal net heating or cooling in the core region. This period coincides with the pre-TT phase, where convection is either weak or spatially disorganized (Fig. 2a). As the TT process begins, a sharp positive spike in $\partial_t\hat{\theta}$ (Eq. (17)) is observed. This

https://doi.org/10.5194/egusphere-2026-1446
Preprint. Discussion started: 30 March 2026

increase is primarily driven by diabatic heating, with an additional positive contribution from the mean heat flux term. This behavior is consistent with the evolution shown in Fig. 1, which highlights a redistribution of PV mainly induced by diabatic latent heat release (Cammas et al., 1994; Hulme and Martin, 2009). In contrast, the eddy heat fluxes contribute negatively during this stage, partially offsetting the positive contributions from the other terms. This suggests that, at the onset of the TT process, diabatic heating and mean flow heat transport dominate over turbulent processes. Shortly thereafter, a pronounced positive spike associated with the turbulent (eddy) heat fluxes emerges, indicating a brief but intense enhancement of heat transport. This signal is likely linked to transient convective bursts that momentarily dominate the heat redistribution within the core, possibly reflecting a period of rapid storm structural reorganization, as documented in previous studies (Gentry et al., 1979; Molinari et al., 1999). Following this turbulent peak, the total heat transport weakens temporarily, before gradually increasing again during the later stages of the TT process. This subsequent intensification is mainly driven by the diabatic heating term, which steadily increases as convection becomes more persistent and organized and the TC approaches a mature structure (Vigh and Schubert, 2009). This evolution is consistent with the establishment of a sustained warm core supported by continuous latent heat release within the developing eyewall region.

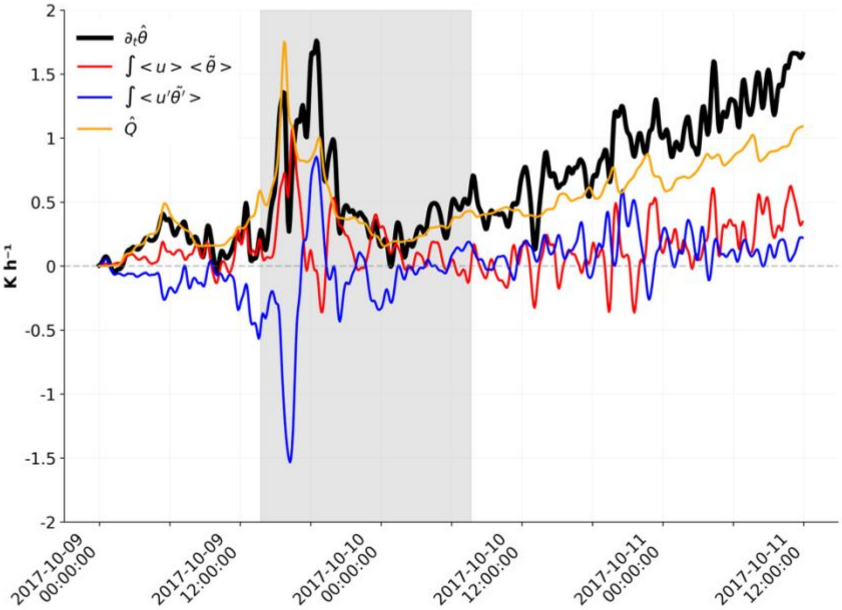

Figure 9: $\frac{\partial\hat{\theta}}{\partial t}$ **(black; K s^{-1}),** $\int_0^H \langle u\rangle\langle\tilde{\theta}\rangle$ **(red),** $\int_0^H \langle u'\tilde{\theta}'\rangle$ **(blue) and** $\hat{Q}$ **(yellow). The gray bar denotes the TT period.**

Figure 10 presents the time-averaged θ budget (Eq. (18)) during the TT period (gray shaded; Fig. 4) at the centre of the cyclone. At the lower levels of the atmosphere, the $\dot{\theta}$ budget is primarily dominated by microphysical processes. This contribution is strongest near the surface and gradually diminishes with height. Starting from around 1000 m altitude, the microphysical tendency begins to decrease steadily and approaches zero by approximately 8000 m. This behavior is associated with the strong

https://doi.org/10.5194/egusphere-2026-1446
Preprint. Discussion started: 30 March 2026

latent heat release at the lower levels (Emanuel, 1986; Hulme and Martin, 2009). The vertical advection term displays a complex vertical structure, characterized by pronounced oscillations throughout the atmospheric column. In the low-mid troposphere, vertical advection increases significantly, contributing positively to the $\dot{\theta}$ budget. This enhancement is closely associated with the presence of deep convection, which plays a critical role in warming the cyclone centre at these levels. In the mid-troposphere, the vertical advection term begins to decline, eventually reaching a local minimum of approximately -0.50×10^{-4} K s^{-1} near 8000 m. In the upper-troposphere, particularly around 11500 m, vertical advection briefly increases to about $+ 0.20 \times 10^{-4}$ K s^{-1}, followed by a sharp dip to a local minimum of nearly $- 1.00 \times 10^{-4}$ K s^{-1} at around 14000 m. From this point upward, it gradually increases again, approaching zero around 18000 m. This pattern in the upper levels aligns with the thermodynamic and dynamic evolution previously commented during the TT. Initially, the system possesses a cold-core structure, but as convection intensifies and latent heat is progressively released, warming initiates near the surface and slowly propagates upward. In the mid-troposphere, warming is more variable and less efficient, leading to the observed oscillations in the vertical advection signal. At upper levels, the emergence of a marked negative advection tendency, indicative of divergence and enhanced upward motion, suggests that air is rising and cooling the upper troposphere. This divergence not only supports continued ascent but also marks the beginning of the transition toward a more tropical-like structure with upper-level outflow and a developing warm core. In contrast, the radiative and turbulent terms contribute minimally to the $\dot{\theta}$ budget across the entire vertical profile. The radiative term shows only minor fluctuations, oscillating slightly between $- 0.05 \times 10^{-4}$ K s^{-1} and 0.00×10^{-4} K s^{-1}. The turbulence term remains essentially constant and close to zero throughout the column.

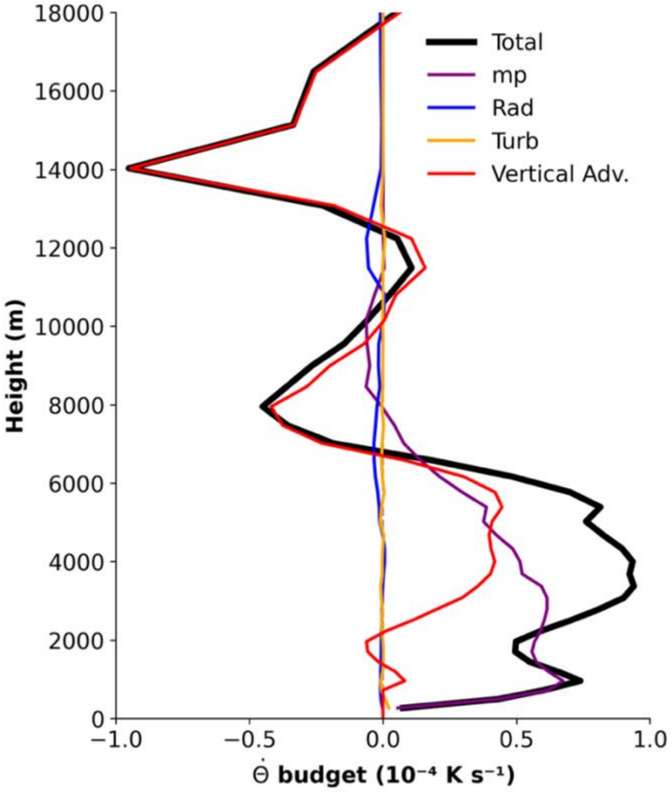

Figure 10: Terms in $\dot{\theta}$ budget (10^{-4}K s^{-1}) during the TT period (gray shaded in Fig. 1) at the centre of the cyclone ($r = 0$ m). Sum of all the $\dot{\theta}$ budget terms (black); tendency from the microphysical scheme (purple); radiation term (blue); turbulence tendency (yellow); and vertical advection (red).

Finally, to synthesize the impact of the dynamic and thermodynamic processes analyzed through the budget equations, Fig. 11 illustrates the resulting structural evolution of the vortex. It presents the time-radius evolution of radial wind at z = 14 km, vertically integrated buoyancy, CAPE and vertical average of positive vertical motion, respectively. Based on the pronounced negative values of the vertical advection term observed at $z = 14$ km in Fig. 10, the evolution of the radial wind at this level is analyzed in Fig. 11a. This upper-tropospheric height is particularly informative for diagnosing the TT process, as it captures the response of the outflow layer to changes in the cyclone dynamical structure. As discussed previously, the development of a strong negative vertical advection tendency at this level is indicative of enhanced divergence aloft and intensified upward motion beneath (Holland and Merrill, 1984), reflecting the strengthening of deep convection. The temporal evolution of the radial wind at 14 km therefore provides valuable insight into the reorganization of the circulation during TT, particularly the establishment and subsequent intensification of the upper-level outflow. Before the TT, the cyclone is predominantly in an upper-level inflow regime, which is also appreciated in Fig. 6 and it is characteristic of its baroclinic nature (Fig. 11a; Guishard et al., 2009). As convection begins to intensify around the surface cyclone, a strong upper-level outflow emerges during the final baroclinic stages and the early TT period. This behavior aligns with Peng et al. (2019), who observed alternating episodes of radial inflow and outflow linked to convective events. Following the mesoscale convective system precursor to the TT, the radial wind continues to oscillate between inflow and outflow phases, contributing to the cyclone intensification through sustained deep convection. Once the system reaches TC category, outflow becomes dominant, which is a signal of the development of the upper-level anticyclone typical of mature TCs (Fig. 11a). In the final stages, a significant inflow is observed, potentially indicating a brief system relaxation and the onset of a new intensification phase.

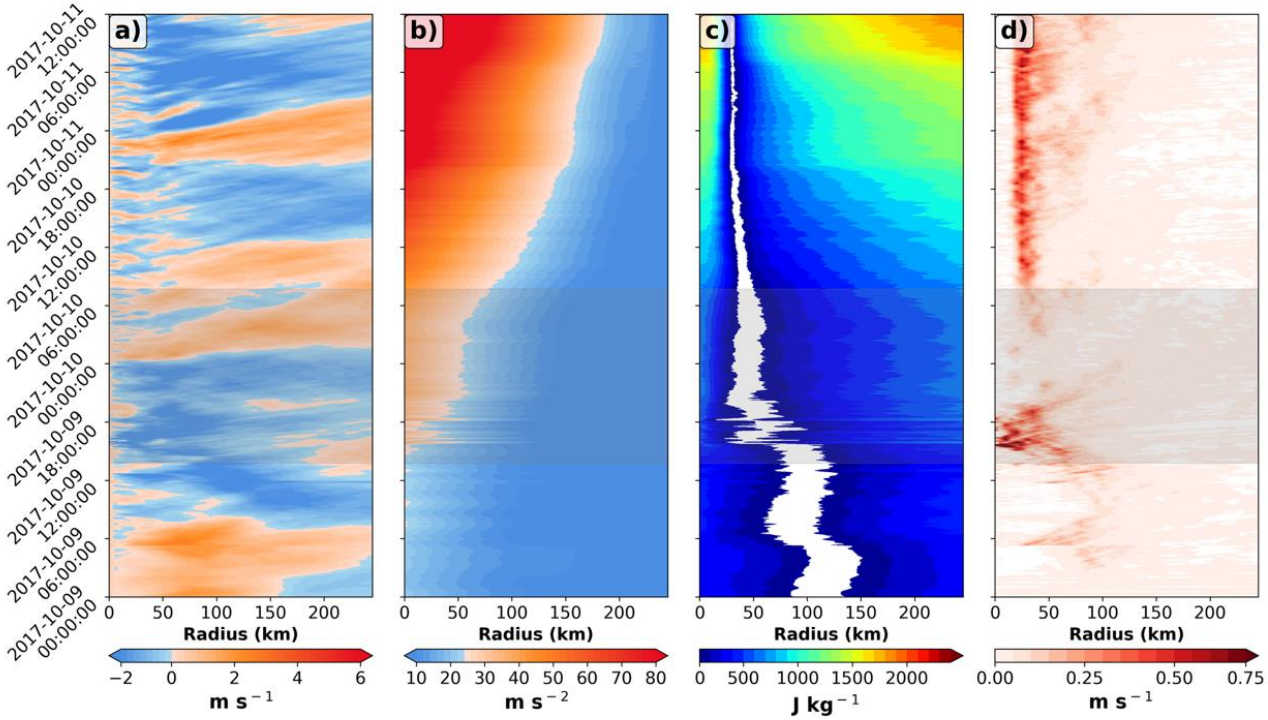

Figure 11: Time-radius azimuthal mean of a) radial velocity (m s^{-1}) at 14 km; b) vertical integral of buoyancy (m s^{-2}); c) CAPE (J kg^{-1}); and d) vertical velocity (m s^{-1}). The gray bar denotes the TT period.

The column-integrated buoyancy in Fig. 11b captures the progressive concentration of latent-heat release that favors the TT in Hurricane Ophelia. In the early period, the buoyancy values are low (< 25 m s^{-2}), consistent with its baroclinic nature and lack of a warm core. As the TT phase develops, enhanced and increasingly organized convection contributes to the formation and subsequent intensification of the warm core. However, the warming core of the system experiences a notable cessation during the TT (≈10 h, Fig. 11b) that is related to the typical system relaxation in subtropical cyclones and TCs that undergo a TT (Davis and Bosart, 2004; Quitián-Hernández et al., 2020). This cessation could be due to a temporary weakening of the secondary circulation associated with structural reorganization, occurring as the system briefly loses baroclinic influence before transitioning to predominantly convective forcing (Quitián-Hernández et al., 2020), which is reflected in several of our diagnostics (Figs. 4-7). Following the system relaxation, buoyancy near the TC centre increases due to a new convection outburst, which facilitates achieving the TT final stage and the vortex gradually intensifies. However, around 2017-10-11

00:00 UTC, the system suffers a new relaxation phase, which is related to the strong inflow atop (Fig. 11a) and it is reflected in the TC eye warming rate (Fig. 8). In this context, internal gravity waves counterbalance the upward buoyant motions associated with convection through downward motions (Lighthill, 1967), propagating from middle to lower tropospheric levels and enhancing the warm core. The thermodynamic effect of this subsidence is evident in Fig. A2f, manifested as a sharp reduction in the moist component due to the downward mixing of drier air. These results are consistent with the findings of Peng et al. (2019) and Calvo-Sancho et al. (2023), who suggest that internal gravity waves redistribute energy, transferring it from the mid to upper troposphere and dispersing it across other tropospheric layers.

The vortex assembles in a weakly unstable environment in the early stages since low CAPE values are in evidence (≈ 200-600 J kg^{-1}), which indicates that no coherent warm-core convection has yet stabilized the column (Fig. 11c; Emanuel, 2003; Molinari et al., 2012). As convective bursts occur during the TT phase (Figs. 11a, b), regions of low CAPE expand, eventually forming a broad area of virtually zero CAPE (white area) within approximately 50–70 km of the centre. After the TT, the low CAPE area collapses close to the TC centre (≈ 40 km), while the surrounding areas rapidly reach high CAPE values (> 1000 J kg^{-1}). This pattern demonstrates that eyewall convection is nearly moist neutral (Emanuel, 1986) and that convective potential exists only in the surrounding region. The surface θ_e flux (Fig. 8) supplies the inflow to the eye and allows the eyewall updraft to release latent heat so that the buoyancy is large while the CAPE is small. This thermodynamic structure is characteristic of a mature TC prepared for the development of secondary rainbands or eyewall cycles (Didlake and Houze, 2013; Kossin and Sitkowski, 2009; Willoughby et al., 1982).

The vertically averaged vertical velocity depicts the reorganization of deep convection that accompanies the TT and favors the development of a pure TC from a baroclinic beginning. Before the TT period, the vertical motions are weak, a structure consistent with baroclinic or shear-dominated precursor disturbances (Davis and Bosart, 2004; Marks and Houze, 1987). During the TT phase, a notable convective burst intensifies and pivots inward, serving as a precursor to the TC and progressively collapsing the primary updraft toward the centre (Fig, 11d). Moreover, this indicates a link between the deep convection and diabatic vortex spin-up via *hot towers* (Montgomery et al., 2006; Rogers et al., 2013). The temporary cessation in warm-core intensification discussed above (Fig. 11b) during the TT is also reflected in the vertical wind field as a brief weakening and redistribution of ascent, indicating reduced net buoyant forcing of the secondary circulation. During this period, the vertical velocity does not intensify but instead exhibits a short pause before strengthening closer to the centre (Fig. 11d). After the TT period, the strongest vertical motion is confined to ≈ 20-40 km, which is related to the eyewall. This is a typical TC mature pattern that supports the secondary circulation required to maintain the warm core (Didlake and Houze, 2013; Hazelton et al., 2017; Peng et al., 2019; Shapiro and Willoughby, 1982).

4. Summary and conclusion

This study is the first explicit analysis of the secondary circulation in a real TT event. It investigates the complex dynamical and thermodynamical mechanisms governing the TT of Hurricane Ophelia (2017), a high-impact event that evolved from a baroclinic environment into a major category 3 hurricane. The co-evolution of the primary and secondary circulations is central to the transformation process. The intensification of the primary vortex is inherently linked to the emergence of a secondary overturning flow. This flow facilitates the necessary radial and vertical transport of energy and momentum required to sustain the transitioning system (Peng et al., 2019). By using high-resolution numerical simulations with the WRF-ARW model and applying rigorous diagnostics of energy budgets and wind tendency equations, this research isolates and quantifies the relative contributions of convective and mesoscale processes in driving the development of the secondary circulation, validating diagnostics techniques previously restricted to idealized simulations and pure tropical cyclones.

The initial synoptic and satellite analysis confirms that Ophelia's genesis was driven by typical baroclinic precursors, specifically a cut-off low and the intrusion of high PV streamers in the upper levels. However, the temporal evolution of the system reveals a fundamental transformation in its vertical structure. Deep convection, initially scattered and asymmetric, progressively organized around the cyclone centre, facilitating the redistribution of PV through diabatic heating. This process resulted in the erosion of upper-level PV and the concentration of PV in the lower troposphere, marking the definitive shift from a cold-core structure to a warm-core vortex sustained by latent heat release. A central finding of this analysis lies in the dynamics of the secondary circulation. During the pre-transition phase, the system is dominated by baroclinic forcing, maintaining a quasi-steady circulation. However, the onset of the TT is characterized by an abrupt and simultaneous increase in the magnitude of the centrifugal and thermal forcing terms; once the transition is complete, the thermal forcing clearly surpasses the countervailing centrifugal and frictional tendencies. This shift indicates that the system successfully transitions to a regime sustained primarily by thermodynamically driven processes, consistent with established theories of TC intensification.

The detailed analysis of the θ and θ_e budgets provide a deeper understanding of the system's internal thermodynamics. The θ budget within the cyclone core demonstrates that diabatic heating is the primary engine of intensification, supported by heat transport via the azimuthal-mean flow. A particularly revealing result is the identification of a significant spike in turbulent eddy heat fluxes at the very beginning of the TT. This feature points to a brief period of structural reorganization dominated by transient convective pulses before sustained diabatic heating takes control of the intensification process. Furthermore, the budget of θ_e in the PBL allows for a clear distinction between the developmental phases. During the TT phase, vertical diffusion, associated with air-sea surface fluxes, is the dominant source of energy, while advective terms have not yet reached their peak magnitude. This indicates that in the early stages, the ocean acts as the critical energy reservoir before the secondary circulation is robust enough to redistribute this energy efficiently. In contrast, during the post-TT phase, vertical advection becomes the dominant mechanism in the eyewall, transporting high entropy from the surface into the free troposphere, a hallmark of mature TCs. The decomposition of the θ_e budget into moist and dry components further reinforces the understanding of this change. While both components contribute comparably during the initial phase, the post-TT phase shows an absolute dominance of the moist component in the advective and diffusive terms within the eyewall. Additionally, a strong negative contribution from radial advection is observed in the mature stage, which can be related to the "ventilation" of the core. This reflects a quasi-equilibrium state where surface heating is balanced by the cooling associated with the secondary circulation and the export of energy to the outer environment.

It is also important to highlight the non-linear behavior of the intensification process observed in the simulations. The results show a temporary cessation in the strengthening of the warm core and secondary circulation midway through the transition. This phenomenon is attributed to a structural adjustment where the system momentarily loses its baroclinic support before becoming fully coupled with convective processes. This underscores the complexity of TT events, suggesting that the pathway to a TC is not always smooth and continuous but involves distinct periods of internal reconfiguration.

In conclusion, the case of Hurricane Ophelia demonstrates that TT is a multi-scale process where the interaction between the initial baroclinic forcing and mesoscale convective *hot towers* is crucial for establishing self-sustaining secondary circulation. The successful transition relies on the capacity of deep convection to redistribute vorticity and establish a warm core, shifting the system from a regime driven by mid-latitude dynamics to one governed by surface enthalpy fluxes and conditional instability. These findings contribute to a better understanding of intensification mechanisms in marginal environments and provide a quantitative framework for future studies on hybrid cyclones in the North Atlantic basin.

Acknowledgements

This work was partially supported by research project PID2023-146344OB-I00 (CONSCIENCE) funded by MICIU/AEI/10.13039/501100011033, the grant PROMETEO CIPROM/2023/38 (DOWNBURST) funded by GVA, and the ECMWF Special Projects (SPESMART, SPESSANC and SPESVALE). R. Rotunno was supported by the NSF under the Cooperative Agreement 1852977. C. Calvo-Sancho acknowledges the grant awarded by the Spanish Ministry of Science and Innovation - FPI program (PRE2020-092343). This research was conducted during the first author visit to NCAR MMM laboratory, which was supported by the research stays aids of FPI program (PRE2020-092343). This work is supported by the CSIC-LINCGLOBAL Ref. LINCG24042; and Interdisciplinary Mathematics Institute of the Complutense University of Madrid.

Competing Interests

The authors declare no conflict of interest. The funding sponsors have no participation in the execution of the experiment, the decision to publish the results, nor the writing of the manuscript.

Author contributions

C.C.S. conceptualized and conducted the research, performed the analysis and drafted the article. R.R. conceptualized and conducted the research, and reviewed the article. A.M.M. conceptualized and conducted the research, performed the analysis and drafted the article. M.L.R. contributed to the research, interpretation of the results and reviewed the article. J.J.G.A. contributed to the research, interpretation of the results and reviewed the article. P.B. reviewed the article and contributed to the research. M.L.M. contributed to the research, supervised the work, reviewed the article and contributed to the interpretation of the results. All authors contributed with editing the manuscript.

Financial support

This work is funded by the Spanish Ministry of Economy under the research project PID2023-146344OB-I00 (CONSCIENCE). This work is also supported by the ECMWF Special Projects SPESMART, SPESSANC and SPESVALE.

References

Bosart, L. F. and Lackmann, G. M.: Postlandfall Tropical Cyclone Reintensification in a Weakly Baroclinic Environment: A Case Study of Hurricane David (September 1979), Mon. Weather Rev., 123, 3268–3291, https://doi.org/10.1175/1520-0493(1995)123%253C3268:PTCRIA%253E2.0.CO;2, 1995.

Bryan, G. H. and Rotunno, R.: The Maximum Intensity of Tropical Cyclones in Axisymmetric Numerical Model Simulations, Mon. Weather Rev., 137, 1770–1789, https://doi.org/10.1175/2008MWR2709.1, 2009.

Calvo-Sancho, C., González-Alemán, J. J., Bolgiani, P., Santos-Muñoz, D., Farrán, J. I., and Martín, M. L.: An environmental synoptic analysis of tropical transitions in the central and Eastern North Atlantic, Atmospheric Res., 278, 106353, https://doi.org/10.1016/j.atmosres.2022.106353, 2022.

Calvo-Sancho, C., Bolgiani, P., Subias, Á., Sastre, M., González-Alemán, J. J., and Martín, M. L.: Horizontal kinetic energy analysis of tropical transition simulations with the WRF and HARMONIE-AROME models, Q. J. R. Meteorol. Soc., 149, 2655–2677, https://doi.org/10.1002/qj.4523, 2023a.

Calvo-Sancho, C., Bolgiani, P., Subias, Á., Sastre, M., González-Alemán, J. J., and Martín, M. L.: Horizontal kinetic energy analysis of tropical transition simulations with the WRF and HARMONIE-AROME models, Q. J. R. Meteorol. Soc., 149, 2655–2677, https://doi.org/10.1002/qj.4523, 2023b.

Cammas, J. P., Keyser, D., Lackmann, G. M., and Molinari, J.: Diabatic redistribution of potential vorticity accompanying the development of an outflow jet within a strong extratropical cyclone, in: Preprints, International Symposium on the Life Cycles of Extratropical Cyclones, Vol. II, International Symposium on the Life Cycles of Extratropical Cyclones, 403–409, 1994.

Cao, X., Wu, R., Jiang, X., Dai, Y., Wang, P., Zhou, L., Wu, L., Deng, D., Sun, Y., Chen, S., Hu, K., Wang, Z., Liu, L., Lan, X., Du, Z., Zhao, J., and Xiao, X.: The southward shift of hurricane genesis over the northern Atlantic Ocean, Npj Clim. Atmospheric Sci., 8, 37, https://doi.org/10.1038/s41612-025-00923-2, 2025.

Davis, C. A.: Simulations of Subtropical Cyclones in a Baroclinic Channel Model, J. Atmospheric Sci., 67, 2871–2892, https://doi.org/10.1175/2010JAS3411.1, 2010.

Davis, C. A. and Bosart, L. F.: Baroclinically Induced Tropical Cyclogenesis, Mon. Weather Rev., 131, 2730–2747, https://doi.org/10.1175/1520-0493(2003)131%253C2730:BITC%253E2.0.CO;2, 2003.

Davis, C. A. and Bosart, L. F.: The TT Problem: Forecasting the Tropical Transition of Cyclones, Bulletin of the American Meteorological Society, 85, 1657–1662, 2004.

Didlake, A. C. and Houze, R. A.: Convective-Scale Variations in the Inner-Core Rainbands of a Tropical Cyclone, J. Atmospheric Sci., 70, 504–523, https://doi.org/10.1175/JAS-D-12-0134.1, 2013.

https://doi.org/10.5194/egusphere-2026-1446
Preprint. Discussion started: 30 March 2026

Dudhia, J.: Numerical Study of Convection Observed during the Winter Monsoon Experiment Using a Mesoscale Two-Dimensional Model, J. Atmospheric Sci., 46, 3077–3107, https://doi.org/10.1175/1520-0469(1989)046%253C3077:NSOCOD%253E2.0.CO;2, 1989.

Eliassen, A.: Slow thermally or frictionally controlled meridional circulation in a circular vortex, Astrophys. Nor., 5, 19–60, 1951.

Emanuel, K.: Tropical Cyclones, Annu. Rev. Earth Planet. Sci., 31, 75–104, https://doi.org/10.1146/annurev.earth.31.100901.141259, 2003.

Emanuel, K. A.: An Air-Sea Interaction Theory for Tropical Cyclones. Part I: Steady-State Maintenance, J. Atmospheric Sci., 43, 585–605, https://doi.org/10.1175/1520-0469(1986)043%253C0585:AASITF%253E2.0.CO;2, 1986.

Emanuel, K. A.: Sensitivity of Tropical Cyclones to Surface Exchange Coefficients and a Revised Steady-State Model incorporating Eye Dynamics, J. Atmospheric Sci., 52, 3969–3976, https://doi.org/10.1175/1520-0469(1995)052%253C3969:SOTCTS%253E2.0.CO;2, 1995.

Evans, J. L. and Hart, R. E.: Objective Indicators of the Life Cycle Evolution of Extratropical Transition for Atlantic Tropical Cyclones, Mon. Weather Rev., 131, 909–925, https://doi.org/10.1175/1520-0493(2003)131%253C0909:OIOTLC%253E2.0.CO;2, 2003.

Galarneau, T. J., McTaggart-Cowan, R., Bosart, L. F., and Davis, C. A.: Development of North Atlantic Tropical Disturbances near Upper-Level Potential Vorticity Streamers, J. Atmospheric Sci., 72, 572–597, https://doi.org/10.1175/JAS-D-14-0106.1, 2015.

Gentry, R. C., Fujita, T. T., and Sheets, R. C.: Aircraft, Spacecraft, Satellite and Radar Observations of Hurricane Gladys, 1968, ournal of Applied Meteorology (1962-1982), 6, 837–850, 1979.

González-Alemán, J. J., Valero, F., Martín-León, F., and Evans, J. L.: Classification and Synoptic Analysis of Subtropical Cyclones within the Northeastern Atlantic Ocean, J. Clim., 28, 3331–3352, https://doi.org/10.1175/JCLI-D-14-00276.1, 2015.

Guisado-Pintado, E. and Jackson, D. W. T.: Coastal Impact From High-Energy Events and the Importance of Concurrent Forcing Parameters: The Cases of Storm Ophelia (2017) and Storm Hector (2018) in NW Ireland, Front. Earth Sci., 7, 190, https://doi.org/10.3389/feart.2019.00190, 2019.

Guishard, M. P., Evans, J. L., and Hart, R. E.: Atlantic Subtropical Storms. Part II: Climatology, J. Clim., 22, 3574–3594, https://doi.org/10.1175/2008JCLI2346.1, 2009.

Hart, R. E., Evans, J. L., and Evans, C.: Synoptic Composites of the Extratropical Transition Life Cycle of North Atlantic Tropical Cyclones: Factors Determining Posttransition Evolution, Mon. Weather Rev., 134, 553–578, https://doi.org/10.1175/MWR3082.1, 2006.

Hazelton, A. T., Rogers, R. F., and Hart, R. E.: Analyzing Simulated Convective Bursts in Two Atlantic Hurricanes. Part I: Burst Formation and Development, Mon. Weather Rev., 145, 3073–3094, https://doi.org/10.1175/MWR-D-16-0267.1, 2017.

Holland, Greg. J. and Merrill, R. T.: On the dynamics of tropical cyclone structural changes, Q. J. R. Meteorol. Soc., 110, 723–745, https://doi.org/10.1002/qj.49711046510, 1984.

Hong, S.-Y. and Lim, J.-O.-J.: The WRF single-moment 6-class microphysics scheme (WSM6), J. Korean Meteorol. Soc., 42, 129–151, 2006.

Hong, S.-Y., Noh, Y., and Dudhia, J.: A New Vertical Diffusion Package with an Explicit Treatment of Entrainment Processes, Mon. Weather Rev., 134, 2318–2341, https://doi.org/10.1175/MWR3199.1, 2006.

Hoskins, B. J., McIntyre, M. E., and Robertson, A. W.: On the use and significance of isentropic potential vorticity maps, Q. J. R. Meteorol. Soc., 111, 877–946, https://doi.org/10.1002/qj.49711147002, 1985.

Hulme, A. L. and Martin, J. E.: Synoptic- and Frontal-Scale Influences on Tropical Transition Events in the Atlantic Basin. Part II: Tropical Transition of Hurricane Karen, Mon. Weather Rev., 137, 3626–3650, https://doi.org/10.1175/2009MWR2803.1, 2009.

Jones, S. C., Harr, P. A., Abraham, J., Bosart, L. F., Bowyer, P. J., Evans, J. L., Hanley, D. E., Hanstrum, B. N., Hart, R. E., Lalaurette, F., Sinclair, M. R., Smith, R. K., and Thorncroft, C.: The Extratropical Transition of Tropical Cyclones: Forecast Challenges, Current Understanding, and Future Directions, Weather Forecast., 18, 1052–1092, https://doi.org/10.1175/1520-0434(2003)018%253C1052:TETOTC%253E2.0.CO;2, 2003.

Kossin, J. P. and Sitkowski, M.: An Objective Model for Identifying Secondary Eyewall Formation in Hurricanes, Mon. Weather Rev., 137, 876–892, https://doi.org/10.1175/2008MWR2701.1, 2009.

Kossin, J. P., Emanuel, K. A., and Vecchi, G. A.: The poleward migration of the location of tropical cyclone maximum intensity, Nature, 509, 349–352, https://doi.org/10.1038/nature13278, 2014.

Landsea, C. W. and Franklin, J. L.: Atlantic Hurricane Database Uncertainty and Presentation of a New Database Format, Mon. Weather Rev., 141, 3576–3592, https://doi.org/10.1175/MWR-D-12-00254.1, 2013.

Lighthill, M.: On waves generated in dispersive systems by travelling forcing effects, with applications to the dynamics of rotating fluids, J. Fluid Mech., 27, 725–752, 1967.

López-Reyes, M., Martín-Pérez, M. L., Calvo-Sancho, C., and González-Alemán, J. J.: Dynamic Forcing Behind Hurricane Lidia's Rapid Intensification, https://doi.org/10.5194/egusphere-2025-3109, 15 August 2025.

Marks, F. D. and Houze, R. A.: Inner Core Structure of Hurricane Alicia from Airborne Doppler Radar Observations, J. Atmospheric Sci., 44, 1296–1317, https://doi.org/10.1175/1520-0469(1987)044%253C1296:ICSOHA%253E2.0.CO;2, 1987.

McTaggart-Cowan, R., Galarneau, T. J., Bosart, L. F., Moore, R. W., and Martius, O.: A Global Climatology of Baroclinically Influenced Tropical Cyclogenesis, Mon. Weather Rev., 141, 1963–1989, https://doi.org/10.1175/MWR-D-12-00186.1, 2013.

Mlawer, E. J., Taubman, S. J., Brown, P. D., Iacono, M. J., and Clough, S. A.: Radiative transfer for inhomogeneous atmospheres: RRTM, a validated correlated-k model for the longwave, J. Geophys. Res. Atmospheres, 102, 16663–16682, https://doi.org/10.1029/97JD00237, 1997.

Molinari, J., Moore, P., and Idone, V.: Convective Structure of Hurricanes as Revealed by Lightning Locations, Mon. Weather Rev., 127, 520–534, https://doi.org/10.1175/1520-0493(1999)127%253C0520:CSOHAR%253E2.0.CO;2, 1999.

Molinari, J., Romps, D. M., Vollaro, D., and Nguyen, L.: CAPE in Tropical Cyclones, J. Atmospheric Sci., 69, 2452–2463, https://doi.org/10.1175/JAS-D-11-0254.1, 2012.

Montgomery, M. T. and Farrell, B. F.: Tropical Cyclone Formation, J. Atmospheric Sci., 50, 285–310, https://doi.org/10.1175/1520-0469(1993)050%253C0285:TCF%253E2.0.CO;2, 1993.

Montgomery, M. T. and Smith, R. K.: Paradigms for tropical cyclone intensification, Aust. Meteorol. Oceanogr. J., 64, 37–66, https://doi.org/10.1071/ES14005, 2014.

Montgomery, M. T., Nicholls, M. E., Cram, T. A., and Saunders, A. B.: A Vortical Hot Tower Route to Tropical Cyclogenesis, J. Atmospheric Sci., 63, 355–386, https://doi.org/10.1175/JAS3604.1, 2006.

Montoro-Mendoza, A., Calvo-Sancho, C., González-Alemán, J. J., Díaz-Fernández, J., Bolgiani, P., Sastre, M., Moreno-Chamarro, E., and Martín, M. L.: Environments conductive to tropical transitions in the North Atlantic: Anthropogenic climate change influence study, Atmospheric Res., 310, 107609, https://doi.org/10.1016/j.atmosres.2024.107609, 2024.

Montoro-Mendoza, A., Calvo-Sancho, C., González-Alemán, J. J., Díaz-Fernández, J., Bolgiani, P., and Martín, M. L.: Strengthening of favorable environments for North Atlantic tropical cyclogenesis in midlatitudes in a warmer climate, Npj Clim. Atmospheric Sci., https://doi.org/10.1038/s41612-025-01317-0, 2026a.

Montoro-Mendoza, A., Calvo-Sancho, C., González-Alemán, J. J., Díaz-Fernández, J., Bolgiani, P., and Martín, M. L.: Strengthening of favorable environments for North Atlantic tropical cyclogenesis in midlatitudes in a warmer climate, Npj Clim. Atmospheric Sci., 9, 45, https://doi.org/10.1038/s41612-025-01317-0, 2026b.

Peng, K., Rotunno, R., Bryan, G. H., and Fang, J.: Evolution of an Axisymmetric Tropical Cyclone before Reaching Slantwise Moist Neutrality, J. Atmospheric Sci., 76, 1865–1884, https://doi.org/10.1175/JAS-D-18-0264.1, 2019.

Quitián-Hernández, L., González-Alemán, J. J., Santos-Muñoz, D., Fernández-González, S., Valero, F., and Martín, M. L.: Subtropical Cyclone Formation via Warm Seclusion Development: The Importance of Surface Fluxes, J. Geophys. Res. Atmospheres, 125, e2019JD031526, https://doi.org/10.1029/2019JD031526, 2020.

Rogers, R., Reasor, P., and Lorsolo, S.: Airborne Doppler Observations of the Inner-Core Structural Differences between Intensifying and Steady-State Tropical Cyclones, Mon. Weather Rev., 141, 2970–2991, https://doi.org/10.1175/MWR-D-12-00357.1, 2013.

Rotunno, R.: Secondary circulations in rotating-flow boundary layers, Aust. Meteorol. Oceanogr. J., 64, 27–35, https://doi.org/10.22499/2.6401.004, 2014.

Rotunno, R. and Emanuel, K. A.: An Air–Sea Interaction Theory for Tropical Cyclones. Part II: Evolutionary Study Using a Nonhydrostatic Axisymmetric Numerical Model, J. Atmospheric Sci., 44, 542–561, https://doi.org/10.1175/1520-0469(1987)044%253C0542:AAITFT%253E2.0.CO;2, 1987.

Sadler, J. C.: The Tropical Upper Tropospheric Trough as a Secondary Source of Typhoons and a Primary Source of Tradewind Disturbances, Air Force Cambridge Research Laboratories, Office of Aerospace Research, Bedford , MA, 55, 1967.

Shapiro, L. J. and Willoughby, H. E.: The Response of Balanced Hurricanes to Local Sources of Heat and Momentum, J. Atmospheric Sci., 39, 378–394, https://doi.org/10.1175/1520-0469(1982)039%253C0378:TROBHT%253E2.0.CO;2, 1982.

Skamarock, W. C., Klemp, J. B., Dudhia, J., Gill, D. O., Liu, Z., Berner, J., Wang, W., Powers, J. G., Duda, M. G., Barker, D. M., and others: A description of the advanced research WRF version 4, NCAR Tech Note Ncartn-556 Str, 145, 2019.

Smith, R. K. and Montgomery, M. T.: Toward Clarity on Understanding Tropical Cyclone Intensification, J. Atmospheric Sci., 72, 3020–3031, https://doi.org/10.1175/JAS-D-15-0017.1, 2015.

Smith, R. K. and Montgomery, M. T.: Understanding hurricanes, Weather, 71, 219–223, https://doi.org/10.1002/wea.2776, 2016.

Stern, D. P. and Nolan, D. S.: On the Vertical Decay Rate of the Maximum Tangential Winds in Tropical Cyclones, J. Atmospheric Sci., 68, 2073–2094, https://doi.org/10.1175/2011JAS3682.1, 2011.

Tang, B. and Emanuel, K.: A Ventilation Index for Tropical Cyclones, Bull. Am. Meteorol. Soc., 93, 1901–1912, https://doi.org/10.1175/BAMS-D-11-00165.1, 2012.

Thorncroft, C. D., Hoskins, B. J., and McIntyre, M. E.: Two paradigms of baroclinic-wave life-cycle behaviour, Q. J. R. Meteorol. Soc., 119, 17–55, https://doi.org/10.1002/qj.49711950903, 1993.

Vecchi, G. A. and Knutson, T. R.: On Estimates of Historical North Atlantic Tropical Cyclone Activity*, J. Clim., 21, 3580–3600, https://doi.org/10.1175/2008JCLI2178.1, 2008.

Vigh, J. L. and Schubert, W. H.: Rapid Development of the Tropical Cyclone Warm Core, J. Atmospheric Sci., 66, 3335–3350, https://doi.org/10.1175/2009JAS3092.1, 2009.

Walsh, K. J. E., Camargo, S. J., Knutson, T. R., Kossin, J., Lee, T.-C., Murakami, H., and Patricola, C.: Tropical cyclones and climate change, Trop. Cyclone Res. Rev., 8, 240–250, https://doi.org/10.1016/j.tcrr.2020.01.004, 2019.

Wernli, H. and Sprenger, M.: Identification and ERA-15 Climatology of Potential Vorticity Streamers and Cutoffs near the Extratropical Tropopause, J. Atmospheric Sci., 64, 1569–1586, https://doi.org/10.1175/JAS3912.1, 2007.

Willoughby, H. E., Clos, J. A., and Shoreibah, M. G.: Concentric Eye Walls, Secondary Wind Maxima, and The Evolution of the Hurricane vortex, J. Atmospheric Sci., 39, 395–411, https://doi.org/10.1175/1520-0469(1982)039%253C0395:CEWSWM%253E2.0.CO;2, 1982.

Zhang, D.-L., Liu, Y., and Yau, M. K.: A Multiscale Numerical Study of Hurricane Andrew (1992). Part III: Dynamically Induced Vertical Motion, Mon. Weather Rev., 128, 3772–3788, https://doi.org/10.1175/1520-0493(2001)129%253C3772:AMNSOH%253E2.0.CO;2, 2000.